Shape transitions in neutron-rich Yb, Hf, W, Os, and Pt isotopes within a Skyrme Hartree-Fock + BCS approach

P. Sarriguren
Instituto de Estructura de la Materia, CSIC, Serrano 123, E-28006 Madrid, Spain

R. Rodríguez-Guzmán
CEA-Saclay DSM/IRFU/SPhN, F-91191 Gif-sur-Yvette, France

L. M. Robledo
Departamento de Física Teórica C-XI, Universidad Autónoma de Madrid, E-28049 Madrid, Spain

(Received 26 March 2008; revised manuscript received 26 May 2008; published 30 June 2008)

Self-consistent axially symmetric Skyrme Hartree-Fock plus BCS calculations are performed to study the evolution of shapes with the number of nucleons in various chains of Yb, Hf, W, Os, and Pt isotopes from neutron number $N = 110$ up to $N = 122$. Potential energy curves are analyzed in a search for signatures of oblate-prolate phase shape transitions, and results from various Skyrme and pairing forces are considered. Comparisons with results obtained with the Gogny interaction as well as with relativistic mean field calculations are presented. The role of the γ degree of freedom is also discussed.

DOI: 10.1103/PhysRevC.77.064322 PACS number(s): 21.60.Jz, 27.70.+q, 27.80.+w

I. INTRODUCTION

The equilibrium shapes that characterize the ground states of atomic nuclei, as well as the transitional regions where shape changes occur, have been the subject of a large number of theoretical and experimental works (for a review, see, for example, Ref. [1] and references therein). In particular, the complex interplay between different competing degrees of freedom, taking place in transitional nuclei, offers the possibility of testing microscopic descriptions of atomic nuclei under a wide variety of conditions. In this context, mean field approximations based on effective interactions with predictive power all over the nuclear chart, which are a cornerstone to almost all microscopic approximations to the nuclear many-body problem, appear as a first theoretical tool to rely on when looking for fingerprints of nuclear phase shape transitions.

Today, systematic mean field studies are possible for two main reasons. First, important advances have been made in the fitting protocols providing effective nucleon-nucleon interactions with predictive power all over the nuclear chart. Popular energy density functionals for calculations along these lines are the nonrelativistic Gogny [2] and Skyrme [3,4] ones, as well as different parametrizations of the relativistic mean field Lagrangian [4,5]. Second, it has also become possible to recast mean field equations in terms of efficient minimizations such as successive iteration methods or the so-called gradient method (see, for example, Refs. [4,6]). The last point is very important when constrained calculations are performed, because, in addition to the usual constraints on both neutron and proton numbers, other external fields could also be added. A typical situation is that in which both β and γ degrees of freedom are taken into account. In addition, mean field approximations are based on product trial wave functions, used to minimize a given energy density functional. Such products break several symmetries of the underlying nuclear Hamiltonian, allowing the use of an enlarged Hilbert space. Within this space, static correlations associated with collective modes (e.g., deformation) are incorporated at the cost of a moderate effort. These are the main reasons why the mean field framework can be considered as a valuable starting point for microscopic nuclear structure studies.

In this paper, we use this approach to gain insight into nuclear shape transitions around ^{190}W. This mass region is particularly interesting, because it lies below doubly magic numbers, and small islands of oblate deformations might be favored energetically. It is also characterized by the strong competition between oblate and prolate configurations (i.e., shape coexistence), and special interest has been given to the case of ^{190}W [7–9]. So far, much data have been collected, especially on the energy spacing of the lowest lying states in even-even systems with mass number $A = 170$–200. Spectroscopic studies on these nuclei have become possible by exploiting the decay of K isomers, which is also a well-known feature characterizing this mass region [10]. This turns into a significant amount of information on the global behavior of these nuclei. For example, the excitation energy of the first 2^+ state is used to correlate the extent of quadrupole deformation, and the ratio of the first 4^+ to the first 2^+ (E_{4^+}/E_{2^+}) can be used, in simple models, to distinguish between an axially symmetric deformed rotor ($E_{4^+}/E_{2^+} = 3.33$), a spherical vibrational nucleus ($E_{4^+}/E_{2^+} = 2.0$), and a triaxial rotor ($E_{4^+}/E_{2^+} = 2.5$) [11,12].

The experimental situation [7,8,13] concerning the ratio E_{4^+}/E_{2^+} for even-even isotopes in this region is summarized in Fig. 1. Clear signatures of shape transitions, which are the main objective of this paper, are visible from this figure. In the left panel, we have plotted the ratio E_{4^+}/E_{2^+} as a function of Z for nine isotone chains from $N = 106$ up to $N = 122$. As can be observed, there is a clear tendency toward the prolate rotational limit ($E_{4^+}/E_{2^+} = 3.33$) in the isotone chains below $N = 116$ as the number of protons decreases. In the case $N = 116$, a change of tendency is also observed between $Z = 76$ (^{192}Os)

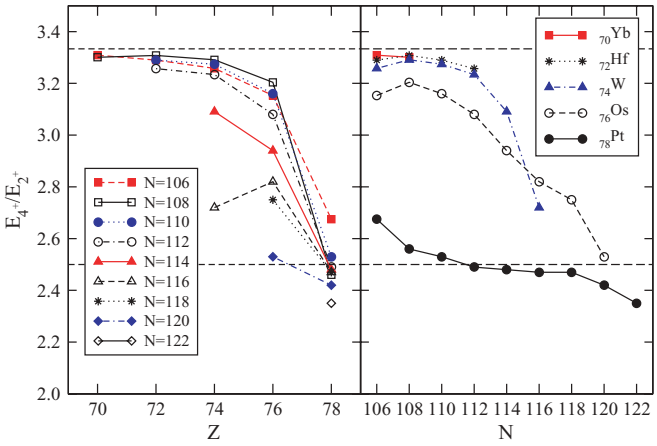

FIG. 1. (Color online) Experimental ratio of the first 4^+ and 2^+ energies for various isotone (left) and isotope (right) chains. Dashed horizontal lines are plotted at 3.33 and 2.5.

and $Z = 74(^{190}\mathrm{W})$, which has been interpreted as a subshell effect [14]. On the other hand, the heavier $N = 116$ isotones ^{192}Os and ^{194}Pt, are well-known examples of γ-soft nuclei [15]; and then it is natural that the γ degree of freedom might also play an important role in ^{190}W, as can be deduced from the close value of the E_{4^+}/E_{2^+} ratio to the 2.5 limit.

In the right panel of Fig. 1, the ratio E_{4^+}/E_{2^+} has been plotted for various isotopes as a function of the neutron number. As can be seen, the lighter Yb, Hf, W, and Os isotopes have a ratio that is very close to the rotational limit. On the other hand, for heavier isotopes, the ratio decreases down to values close to 2.5, and the tendency is to continue toward the spherical limit. Finally, the Pt isotopes have ratios that indicate a pronounced γ-soft character.

From the theoretical point of view, a shape transition from prolate to oblate as the number of neutrons is increased in this mass region has been predicted by different models [15–20]. For instance, a pioneer study within the shell correction method with a deformed Woods-Saxon potential and monopole pairing interaction has been used [16] to discuss the prolate-oblate shape change in Os isotopes. It has been found that the shape change takes place between $N = 114$ and $N = 116$, while similar studies [17] based on total Routhian surface calculations also suggested this transition to occur at $N = 118$. On the other hand, various collective models were tested in Ref. [15] to describe the $E2$ properties of the low-lying states in several rare-earth Os and Pt isotopes. The results indicated that the data were consistent with the description of these nuclei as being γ soft. Shape predictions from relativistic and nonrelativistic studies with angular momentum projection for Hf, W, and Os isotopes were also compared in Ref. [18]. While relativistic calculations predicted a majority of prolate shapes, cycling changes in the sign of the quadrupole parameters were observed in the case of nonrelativistic calculations. More recently, the shape transition in both Os and Pt isotopes has been studied within the relativistic mean field (RMF) approximation using the parametrization NL3, which is perhaps the best parameter set ever fitted for the RMF Lagrangian, together with a finite range Brink-Boeker pairing interaction [19] and also within a nonrelativistic self-consistent axially deformed Hartree-Fock (HF) framework based on a separable monopole interaction [20,21].

Nevertheless, and to the best of our knowledge, no systematic study of shape transitions in this mass region has been carried out yet within the framework of Skyrme Hartree-Fock calculations with pairing correlations, which is at present one of the state-of-the-art mean field descriptions (see, for example, Refs. [3,4,22]). Therefore, in this work we study the ground state shape evolution in five isotopic chains, namely, Yb, Hf, W, Os, and Pt from $N = 110$ up to $N = 122$ in an attempt to get the first hints of nuclear shape transitions for these nuclei. In particular, we will first keep axial symmetry as a self-consistent symmetry [23] and construct potential energy curves (PECs) as functions of the (axially symmetric) mass quadrupole moment for the above-mentioned chains of nuclei. These PECs are obtained from the corresponding constrained Skyrme Hartree-Fock + BCS calculations, using the forces Sk3 [24], SLy4 [25], and SLy6 [25] in the particle-hole channel and different recipes for pairing correlations. The axially symmetric calculations should be regarded as a first step and will allow us to disentangle the sensitivity of our predictions with respect to the method employed to solve the deformed HF+BCS equations (i.e., discretization in a Cartesian mesh or expansion into an axially symmetric harmonic oscillator basis), as well as to the effective Skyrme and pairing interactions. Additionally, we will compare our findings with the results obtained with the parametrization D1S [26] of the Gogny interaction [2]. Let us remark that the main intention in this work is to obtain the first hints of shape transitions around the nucleus ^{190}W using effective forces whose predictive power has already been shown when describing ground state nuclear properties all over the nuclear chart. In this context, the set of effective interactions already mentioned is well suited, and it is very interesting to compare their predictions.

In a second step, the role played by the γ degree of freedom will be discussed. The corresponding triaxial calculations will be based on the code EV8 [22], our main computational tool in the present work. We will take advantage of its three-dimensional lattice discretization, which allows us to treat any quadrupole deformation effect, axial or triaxial, on the same footing [4,27]. On the other hand, these calculations are much more involved than the axial ones (about a factor of 60 much more expensive in computing time) and therefore have been restricted to a relevant sample of nuclei in the present study.

The paper can be outlined as follows. In Sec. II, we briefly describe the main theoretical formalism (Hartree-Fock + BCS) used to obtain the main ingredients of the present study, i.e., the PECs and potential energy surfaces (PESs) for the considered isotopic chains. For more details, the reader is referred to the corresponding literature. Section III contains our results. There, we first discuss the sensitivity of the PECs (obtained in the framework of axially symmetric calculations) to the effective nucleon-nucleon force and to the treatment of the pairing correlations; in a second step, the role of triaxiality (i.e., the γ degree of freedom) will be illustrated for nuclei of the Yb, Hf, W, Os, and Pt chains with neutron numbers

$N = 114$, 116, and 118. Finally, Sec. IV is devoted to the concluding remarks and work perspectives.

II. THEORETICAL FRAMEWORK

Our microscopic approach is based on a self-consistent formalism built on a deformed Hartree-Fock mean field, using Skyrme-type two-body interactions, plus pairing correlations between like nucleons included in the BCS approximation. As is well known, the density-dependent HF+BCS approximation provides a very good description of ground state properties for both spherical and deformed nuclei [27], and it is at present one of the possible state-of-the-art mean field descriptions [4].

We have used two methods of solving the deformed HF+BCS equations. The first method is based on the expansion of the single-particle wave functions into an appropriate orthogonal basis (the eigenfunctions of an axially symmetric harmonic oscillator potential), following the procedure based on the formalism developed in Ref. [3]. The second method, which is our main choice for the calculations performed in this study, uses a coordinate space mesh, solving the HF+BCS equations for Skyrme-type functionals via discretization of the individual wave functions on a three-dimensional Cartesian mesh [22]. As a matter of fact, it can be shown that this corresponds to an expansion on the basis of Lagrange polynomials associated with the selected three-dimensional mesh [28]. One of the main advantages of the three-dimensional discretization is that any quadrupole deformation effect, axial or triaxial, can be taken into account on the same footing [4,27]. As a result, this second method represents our main computational tool in the present study and will be used later on when examining the role played by the γ degree of freedom for the considered nuclei.

We have mainly considered three different parametrizations of the effective Skyrme-like interactions in the particle-hole channel. As the leading choice, we have performed calculations (both axial and triaxial) with the parametrization SLy4 [25]. We also show results in some instances (i.e., at the level of axially symmetric calculations) for the Skyrme forces Sk3 [24] and SLy6 [25]. They are examples of global effective Skyrme interactions that have been designed to fit ground state properties of spherical nuclei and nuclear matter properties. While Sk3 is the simplest one, involving in particular a linear dependence on the density, the Lyon force SLy4 represents a parametrization obtained with a more recent fitting protocol, and its predictive power has already been shown to be very reasonable all over the nuclear chart [4]. Calculations have also been performed with the Skyrme parameter set SLy6, which includes additionally a two-body center-of-mass correction in the corresponding energy functional.

As a first step, HF+BCS calculations preserving axial symmetry have been performed using the Skyrme forces mentioned above. Our plan is, on the one hand, to use the axially symmetric calculations to study the sensitivity of our results to the effective interactions used in the particle-hole and pairing channels. On the other hand, we will also use them to obtain, in the framework of our Skyrme HF+BCS study, first hints of shape transitions around ^{190}W. Obviously, pairing correlations have also been taken into account, and we have selected a zero-range density-dependent pairing force [29],

$$V(\mathbf{r_1}, \mathbf{r_2}) = -g(1 - \hat{P}^{\sigma}) \left(1 - \frac{\rho(\mathbf{r_1})}{\rho_c}\right) \delta(\mathbf{r_1} - \mathbf{r_2}), \quad (1)$$

as our leading choice in the particle-particle channel. In Eq. (1), $\hat{P}^{\sigma}$ is the spin exchange operator, $\rho(\mathbf{r})$ is the nuclear density, and $\rho_c = 0.16$ fm^{-3}. The strength g of the pairing force [Eq. (1)] is taken $g = 1000$ MeV fm^3 for both neutrons and protons, and a smooth cutoff of 5 MeV around the Fermi level has been introduced [29,30]. Let us mention that very recently, the parametrization SLy4 has been successfully applied in combination with the pairing interaction [Eq. (1)] (with $g = 1000$ MeV fm^3) in systematic studies of correlation energies from ^{16}O to the superheavies [31] and in global studies of spectroscopic properties of the first 2^+ states in even-even nuclei [32]. Thus, the predictive power of this combination of effective interactions has been well established along the nuclear chart, and this is the main reason for selecting the combination SLy4 in the particle-hole channel and the interaction of Eq. (1) (with $g = 1000$ MeV fm^3) in the pairing channel as the leading choice for the present study. Calculations with the parametrization SLy6 in the particle-hole channel and the interaction of Eq. (1) (with $g = 1000$ MeV fm^3) have also been performed.

In this work, we also consider other recipes for pairing correlations. For example, a schematic seniority pairing force with a constant pairing strength G parametrized to reproduce the phenomenological pairing gaps will also be used. This treatment is called constant-force approach. One can also further simplify the pairing treatment by parametrizing the pairing gaps $\Delta_{p,n}$ directly from experiment, we call this treatment the constant-gap approach. The pairing strength G and the pairing gap are related through the gap equation [23]

$$\Delta = G \sum_{k>0} u_k v_k, \quad (2)$$

where v_k are the occupation amplitudes ($u_k^2 = 1 - v_k^2$).

The PECs shown later in this paper (see Sec. III) are computed microscopically by constrained HF+BCS calculations [23,33] in which axial symmetry is kept as self-consistent symmetry [23] during the typical mean field iterative procedure [4].

In a second step, calculations exploring the role played by the γ degree of freedom have been performed [22] for the Yb, Hf, W, Os, and Pt chains with neutron numbers $N = 114$, 116, and 118. As mentioned before, the triaxial calculations are more involved than the axial ones, and we have restricted them to that selected set of nuclei. As in the axially symmetric calculations, the corresponding energy functional is minimized under a quadratic constraint that holds the mass quadrupole moment fixed to a given value (expressed in barns) [22,23] and the nonlinear HF+BCS equations are solved using the method of successive iterations [4,22]. In addition to the usual mean field constraints on both neutron and proton numbers, the nuclear shape is determined by constraining simultaneously the pair of values (q_1, q_2) related with the parameters Q and γ

through the equations [22]

$$q_1 = Q\left(\cos\gamma - \frac{1}{\sqrt{3}}\sin\gamma\right),$$
$$q_2 = Q\frac{2}{\sqrt{3}}\sin\gamma, \qquad (3)$$
$$Q = \sqrt{q_1^2 + q_2^2 + q_1 q_2}.$$

Particular shapes of interest are the prolate ones with $\gamma = 0°(q_1 = Q, q_2 = 0)$ and the oblate ones with $\gamma = 60°(q_1 = 0, q_2 = Q)$, while triaxial shapes lie in between them. Using chains of triaxial calculations, we have checked the stability of the minima predicted in the framework of the axially symmetric calculations (first step in the present study) with respect to the γ degree of freedom. These calculations will also be discussed in Sec. III and have been performed with the parametrization SLy4 plus the pairing interaction of Eq. (1) (with $g = 1000$ MeV fm^3).

III. DISCUSSION OF RESULTS

In this section, we will discuss the results obtained in our study. First, we will discuss those obtained with the restriction to axially symmetric shapes; then, in a second step, we will illustrate the role played by the γ degree of freedom.

As is well known, PECs are sensitive to the effective nuclear force in both relativistic [34] and nonrelativistic [35,36] approaches, as well as to pairing correlations [35–37]. Thus, we begin our discussion on the PECs by considering sample results in order to study the sensitivity of our predictions to effective interactions in both the particle-hole and the pairing channels. In Fig. 2 we consider the PECs obtained in the

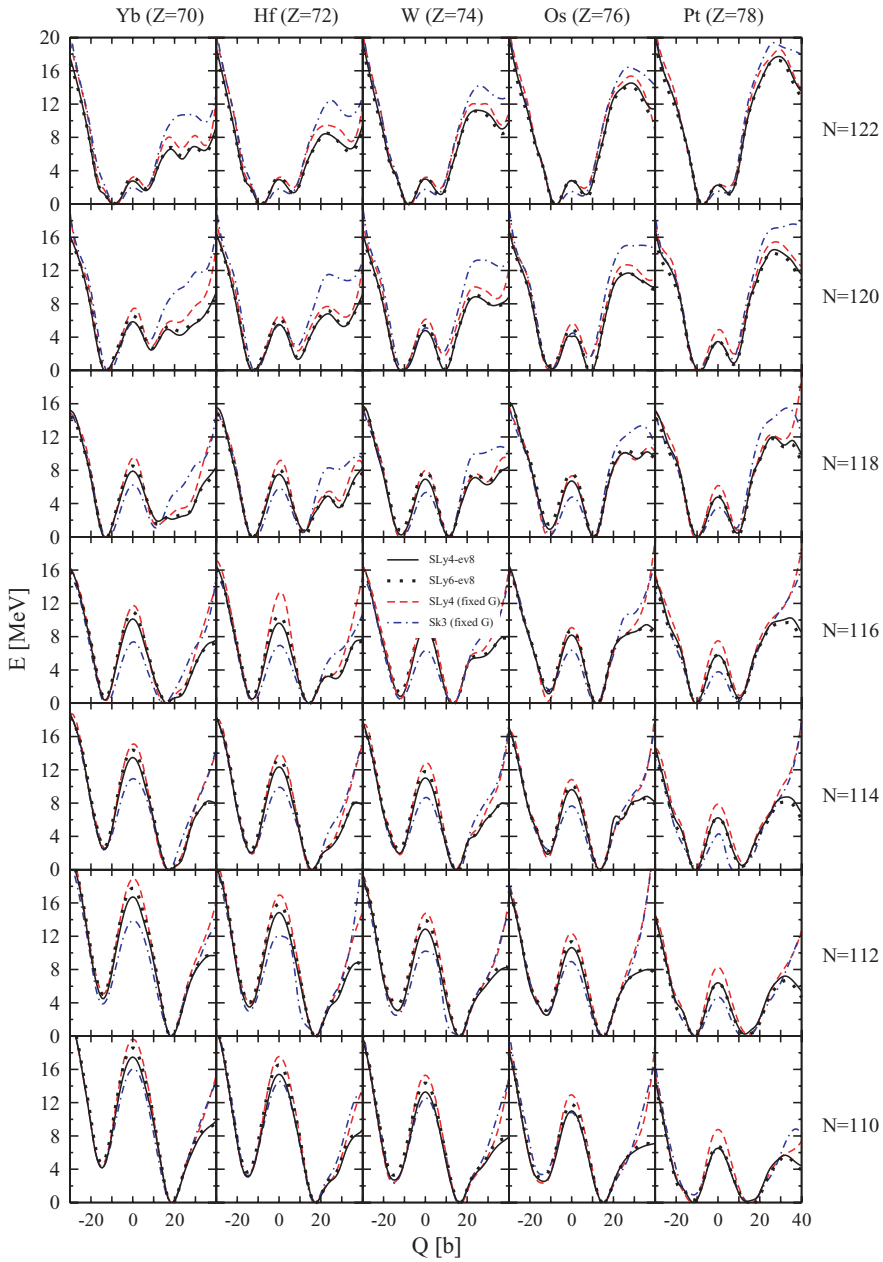

FIG. 2. (Color online) PECs for several isotope chains obtained from HF+BCS calculations with various Skyrme and pairing forces.

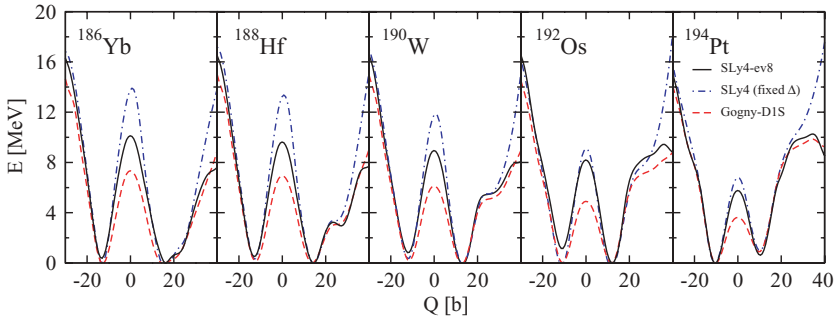

FIG. 3. (Color online) PECs for $N = 116$ isotones obtained from mean field calculations with various forces.

framework of the axially symmetric calculations described in Sec. II with the Skyrme forces Sk3, SLy4, and SLy6 and various pairing treatments. Taking as a reference the results obtained from the most sophisticated method based on the coordinate space mesh calculation [22] with the forces SLy4 and SLy6 plus a zero-range density-dependent pairing force with strength $g = 1000$ MeV fm^3, labeled SLy4-ev8 (solid lines) and SLy6-ev8 (dotted lines) in the figure, one can see that the results do not differ much when changing the pairing treatment to a constant-force approach (dashed lines) or when changing the Skyrme interaction into Sk3 (dash-dotted lines). It can also be seen that the locations of the oblate and prolate minima appear at the same deformations, no matter what the force is. However, the relative energies can be slightly different, and the spherical energy barriers between the prolate and oblate minima of the PECs can change by a few MeV, depending on the force. In general, the energy barriers at zero deformation are lower with the force Sk3 and the delta pairing force also makes the barriers somewhat lower. These results indicate that the topology of the PECs is sensitive to the details of the calculations, as has already been pointed out in Ref. [37]. Additionally, Fig. 2 clearly shows that at least for some of the nuclei considered, there is a very strong competition between different low-lying configurations corresponding to different intrinsic deformations (i.e., shape coexistence), and therefore dynamical correlations not explicitly taken into account at the mean field level (for example, symmetry restoration and/or configuration mixing) could certainly play a role in the description of ground state properties in these nuclei.

If one analyzes Fig. 2 in the vertical direction along isotope chains, one can see a clear evolution from prolate to oblate shapes for increasing neutron number. This transition takes place at $N = 116$ in Yb and Hf isotopes and at $N = 116$ and $N = 118$ in W and Os isotopes, and it is a very soft transition in Pt isotopes. On the other hand, horizontally along isotone chains and except for the Pt isotopes, the isotones with $N = 122, 120$, and 118 are oblate, while those with $N = 114, 112$, and 110 are prolate. Isotones with $N = 116$ are transitional nuclei with oblate and prolate minima at about the same energy and therefore showing a more pronounced shape coexistence. It is also worth noticing that the energy barriers at zero deformation decrease almost linearly with the number of protons as Z increases in a given isotone chain. The same reduction is observed in isotope chains as N increases.

The previous results are in qualitative good agreement with the ones obtained in Ref. [19] using the parametrization NL3 of the RMF Lagrangian and a pairing force based on the Brink-Boeker part of the Gogny interaction. The energy barriers are found to be lower than SLy4, but the location of the equilibrium deformations does not change much. The agreement of our results with those in Ref. [20] is also satisfactory concerning the location of the minima, but the energy barriers at zero deformation are clearly lower in that reference. In general, our results are in good agreement with those obtained in previous studies. However, the nuclides at which the transitions from one shape to another take place may change because of the small energy differences between the oblate and prolate minima in the transitional region.

Figures 3 and 4 show a comparison of the PECs obtained from the force SLy4 and a zero-range density-dependent pairing force (referred as SLy4-ev8) with those obtained from Hartree-Fock-Bogoliubov calculations [38,39] based on the parametrization D1S of the Gogny interaction [26]. As is well known, the advantage of the Gogny interaction over other alternatives is that its finite range allows a fully self-consistent treatment of pairing correlations with the same interaction that produces, due to its structure, the proper cutoff for the pairing matrix elements.

The comparison in Fig. 3 is for the isotone chain $N = 116$, while a similar comparison in Fig. 4 is for the isotope chain $Z = 74$. Figure 3 also gives the results obtained with the Skyrme force SLy4 using a simple constant-gap approach

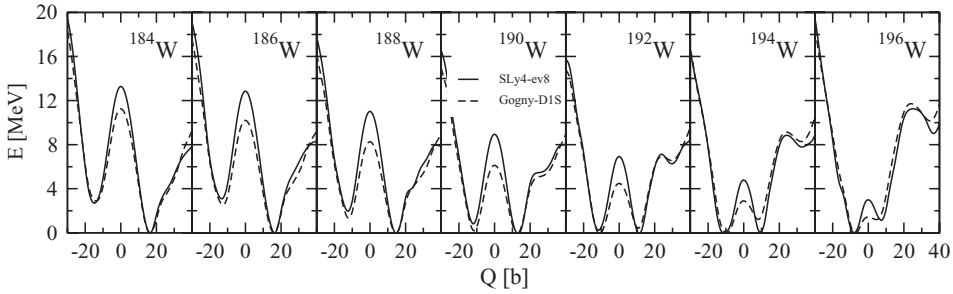

FIG. 4. PECs for $Z = 74$ isotopes obtained from mean field calculations with various forces.

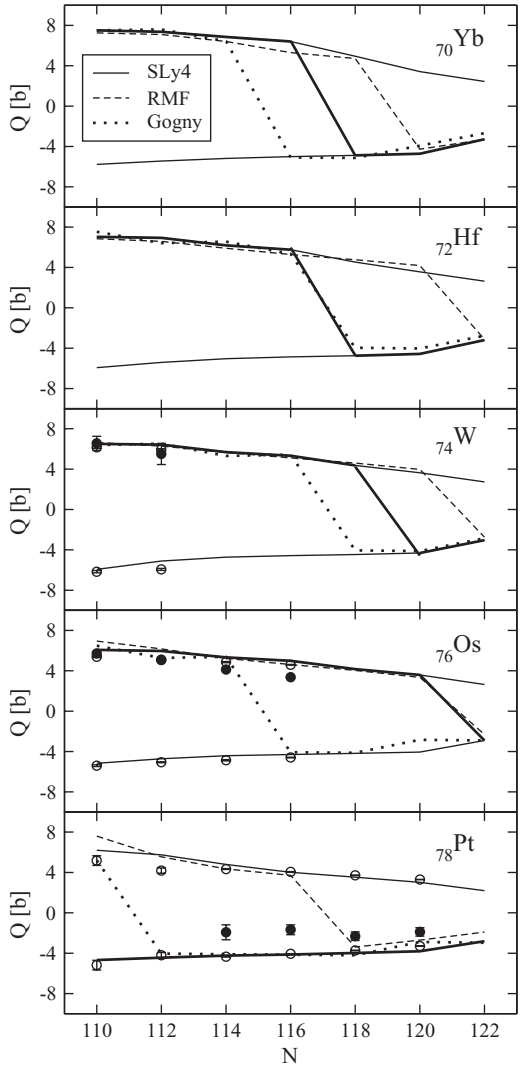

FIG. 5. Intrinsic quadrupole moments for five isotope chains as a function of neutron number. Theoretical results obtained from Skyrme-SLy4, relativistic mean field (RMF), and Gogny force are compared with experimental data from Refs. [42] (full circles) and [43] (open circles). For SLy4, thick lines connect the quadrupole moments of the ground states.

in the pairing channel with pairing gaps obtained from the experimental masses of neighboring nuclei [40]. These figures show again that the location of the minima is rather stable at practically the same deformations. It should also be noted that the energy barriers are somewhat lower with the Gogny interaction and somewhat larger with the constant-gap approach.

The quadrupole moments of the charge distributions of these nuclei can be compared with the available experimental information. This is done in Fig. 5 for our five isotopic chains as a function of the neutron number. Our theoretical results obtained from SLy4 are shown by thin solid lines, one connecting the prolate minima and the other joining the oblate ones. Thick lines connect the quadrupole moments corresponding to the ground states of the nuclei. We also show by dashed lines the quadrupole moments of the ground states obtained from RMF calculations [41] (parametrization NL3) and the BCS formalism with constant pairing gaps. Dotted lines correspond to Gogny-D1S calculations [39]. Experimental data (full circles) are taken from the most updated compilation of available data on static nuclear electric quadrupole moments [42], transforming the laboratory quadrupole moments corresponding to the first 2^+ excitations into intrinsic ones by using $Q_{\rm intr} = -3.5\, Q_{\rm lab}$. We also show the experimental intrinsic quadrupole moments derived from the experimental values of $B(E2)$ strengths [43]. In this case, the sign cannot be extracted and therefore we show by open circles in Fig. 5 both possibilities of signs. Actually, the $B(E2)$ strengths are converted into quadrupole moments [43] under the assumption of a well-defined axial rotor behavior that in our case can be identified with values of the E_{4^+}/E_{2^+} ratio close to 3.33. It is worth noticing that in Ref. [15] a complete set of $E2$ matrix elements involving the low-lying excited states in ^{186,188,190,192}Os and ^{194}Pt was measured. This includes not only the $B(E2)$ values but also the relative signs between the transitional $E2$ matrix elements and the static quadrupole moments. In particular, it was shown that the $\langle Q^2 \rangle$ centroids are nearly spin independent, suggesting that the $E2$ properties are correlated and that the collective motion is rotation-like. The general trend of the data in Ref. [15] is consistent with the description in terms of γ-soft type collective models through a prolate to oblate shape transition. It would be very interesting in the future to include dynamical correlations beyond the static mean field picture used in this work and compare the results with those data.

As can be observed from Fig. 5, there is a nice agreement between our SLy4 results and the experimental ones, including the sign (full circles). At the same time, RMF calculations fail to describe the sign of ^{192,194}Pt isotopes, while calculations with the Gogny interaction fail to describe the quadrupole moment of ^{192}Os. Nevertheless, one should notice that in the transitional region, this discrepancy is not very significant, because the energies corresponding to the two deformations are practically the same and small details of the calculation may change the relative energy difference between the oblate and prolate shapes.

Finally, we show in Table I the moments of inertia calculated microscopically within the cranking model, as well as the moments of inertia from various macroscopic models,

TABLE I. Ratio E_{4^+}/E_{2^+} and moments of inertia $\mathcal{I}$ (MeV $^{-1}$) obtained from the first experimental 2^+ energy ($\mathcal{I}_{\rm exp}$), from a cranking calculation with SLy4 ($\mathcal{I}_{\rm SLy4}$) and Gogny ($\mathcal{I}_{\rm Gogny}$), as well as from macroscopic descriptions of the nucleus as an irrotational flow ($\mathcal{I}_{\rm i.f.}$) and a rigid rotor ($\mathcal{I}_{\rm r.r.}$). Only nuclei with $E_{4^+}/E_{2^+} > 3$ are considered.

	E_{4^+}/E_{2^+}	$\mathcal{I}_{\rm exp}$	$\mathcal{I}_{\rm SLy4}$	$\mathcal{I}_{\rm Gogny}$	$\mathcal{I}_{\rm i.f.}$	$\mathcal{I}_{\rm r.r.}$
^{182}Hf	3.29	30.7	31.8	31.5	5.0	87.9
^{184}Hf	3.26	27.9	33.6	35.0	4.8	89.4
^{184}W	3.27	27.0	30.0	27.6	4.3	89.0
^{186}W	3.23	24.5	32.0	32.5	4.1	90.4
^{188}W	3.09	21.0	33.0	23.3	3.2	91.3
^{186}Os	3.16	21.9	29.2	26.8	3.8	90.2
^{188}Os	3.08	19.4	31.6	23.5	3.6	91.6

namely, the rigid rotor ($\mathcal{I}_{\text{r.r.}}$) and the irrotational flow ($\mathcal{I}_{\text{i.f.}}$) models. The expressions used to calculate the moments of inertia can be found in Refs. [23,44]:

$$\mathcal{I}_{\text{cranking}} = 2 \sum_{k,k'>0} \frac{|\langle k|J_x|k'\rangle|^2}{E_k + E_{k'}} (u_k v_{k'} - u_{k'} v_k)^2, \quad (4)$$

$$\mathcal{I}_{\text{r.r.}} = \frac{2}{5} m A R_0^2 \left(1 + \sqrt{\frac{5}{16\pi}}\beta\right), \quad (5)$$

$$\mathcal{I}_{\text{i.f.}} = \frac{3}{5} \rho_0 R_0^5 \beta^2. \quad (6)$$

In these expressions, β is the quadrupole deformation defined in terms of the mass quadrupole moment Q and the mean-square radius of the mass distribution $\langle r^2 \rangle$,

$$\beta = \sqrt{\frac{\pi}{5}} \frac{Q}{A\langle r^2 \rangle}. \quad (7)$$

We compare our results with the experimental moments of inertia extracted from the first 2^+ excitations under the assumption that they correspond to rotors with $E_{2^+} = 3/\mathcal{I}$ [23]. Thus, we quote only those nuclei with ratios E_{4^+}/E_{2^+} close to the value 3.33. As expected, the rigid rotor and irrotational flow models predict, respectively, upper and lower limits to the phenomenological moment of inertia. The cranking moments of inertia, calculated either with SLy4 or Gogny forces, are much closer to experiment.

Let us now turn to the second part of our discussion, i.e., the role played by the γ degree of freedom in the considered nuclei. That triaxiality could certainly play a role for nuclei in this region of the nuclear chart becomes already clear if one keeps in mind that the heavier $N = 116$ isotones ^{192}Os and ^{194}Pt are known to be γ-soft nuclei [15]. The same applies to ^{190}W from its E_{4^+}/E_{2^+} ratio approaching the limit of 2.5 (see Fig. 1). Therefore, to confirm the reliability of the shape transitions predicted in the framework of the axially symmetric calculations discussed above, we carried out calculations constraining the Q-γ degrees of freedom (instead of the β deformation parameter, we use the Q quadrupole moment) along the lines described in Sec. II. The calculations in Figs. 6 and 7 have been performed with the parametrization SLy4 in the particle-hole channel plus the pairing interaction [Eq. (1)] with $g = 1000$ MeV fm^3.

In Fig. 6, the contour plot for the PES of the nucleus ^{190}W is presented. From this figure, we immediately realize that the nucleus ^{190}W has a triaxial ground state whose coordinates in the Q-γ plane are $(Q, \gamma) = (14\,\text{b}, 25^\circ)$. The figure shows a soft behavior on the γ degree of freedom with a very shallow triaxial minimum, which lies less than 0.5 (1.3) MeV below the prolate (oblate) minimum. To gain a better insight into the role of triaxiality in this mass region, we performed similar calculations for other Yb, Hf, W, Os, and Pt nuclei with neutron numbers $N = 114$, 116, and 118. The results of these calculations are summarized in Fig. 7, which plots the HF+BCS energy as a function of the triaxial deformation parameter γ (in degrees) for the Q values at which the energy minima are obtained in the axial case. In general, we can see that the oblate and prolate minima are connected in the γ variable with smooth functions exhibiting in some cases

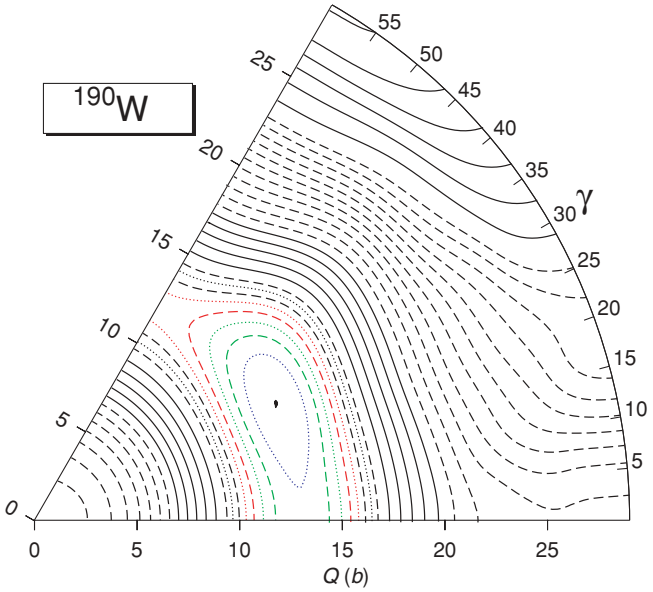

FIG. 6. (Color online) Contour plot of the PES of ^{190}W in a β-γ plane-like representation. Instead of the β deformation parameter, we used the total mass quadrupole moment Q [see Eq. (3)] in units of barns. γ is in degrees. The contour lines correspond to the following scheme: from $\epsilon_{\text{min}} + 0.25$ MeV to $\epsilon_{\text{min}} + 2.0$ MeV alternating dotted and dashed contours are plotted every 0.25 MeV (the contour $\epsilon_{\text{min}} + 0.25$ MeV is plotted in blue, the contours $\epsilon_{\text{min}} + 0.50$ MeV and $\epsilon_{\text{min}} + 0.75$ MeV are plotted in green; those corresponding to $\epsilon_{\text{min}} + 1.00$ MeV and $\epsilon_{\text{min}} + 1.25$ MeV are plotted in red; the rest in black); from $\epsilon_{\text{min}} + 2.50$ MeV to $\epsilon_{\text{min}} + 4.50$ MeV the contour lines are plotted every 0.50 MeV as full lines; from $\epsilon_{\text{min}} + 5.00$ MeV to $\epsilon_{\text{min}} + 10.00$ MeV the contour lines are plotted again every 0.50 MeV as dashed lines; finally from $\epsilon_{\text{min}} + 11.00$ MeV to $\epsilon_{\text{min}} + 20.00$ MeV contour lines are depicted every 1.00 MeV as full lines. Calculations have been performed with the parametrization SLy4 of the Skyrme force in the particle-hole channel plus a zero range and density-dependent pairing interaction with strength $g = 1000$ MeV fm^3.

shallow local minima or low peaks. The barriers found are of the order of a few hundred keV, much lower than the typical spherical barriers in the β variable, which can reach values up to 20 MeV, depending on the example (see Fig. 2). For the Yb and Hf isotopes, we can see a transition from prolate ($N = 114$) to oblate ($N = 118$) shapes, passing through a γ-soft isotope ($N = 116$), which shows smooth peaks and valleys. We also observe that in these two isotopes, one of the axial minima, oblate in $N = 114$ and $N = 116$ and prolate in $N = 118$, is indeed a saddle point, unstable in the γ direction. For W isotopes, we can see that the axial prolate and oblate minima are again connected through soft curves in the γ direction, allowing for triaxial minima; this is especially clear in the $N = 118$ isotone. The oblate minima in β become saddle points when the γ degree of freedom is considered. The same happens for the $N = 116$ and $N = 118$ prolate minima. Finally, Os (Pt) isotopes are examples of very soft prolate (oblate) nuclei with axial minima separated by about 1 MeV and connected through extremely shallow triaxial minima. Again, the oblate minima become saddle points, and this is also

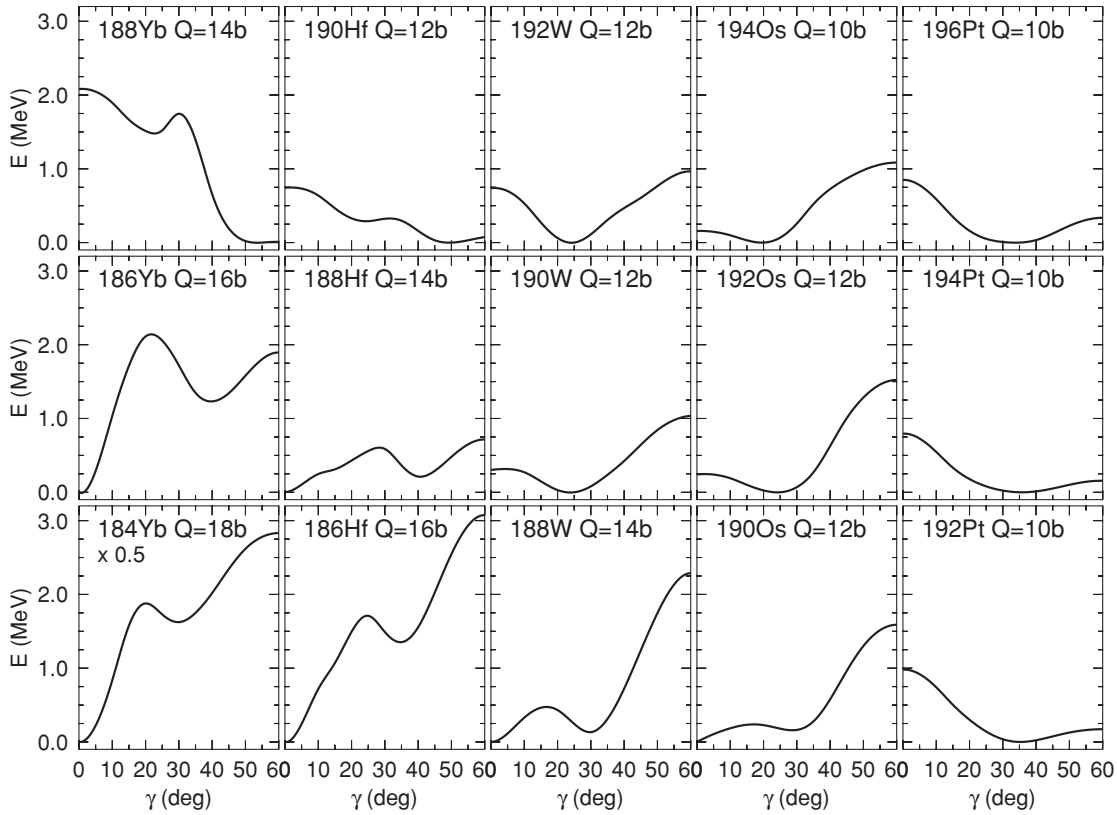

FIG. 7. HF+BCS energy of $N = 114$, 116, and 118 isotones plotted as a function of the triaxial deformation parameter γ (degrees) for the Q values at which the energy minima are obtained in the axial case.

the case for the prolate ones, with the exception of ^{190}Os. It is worth noticing once more that the axial minima are separated by spherical energy barriers ranging between 5 and 10 MeV. The general trend seems to be quite clear: whenever there is a minimum which is much deeper than the other (2 MeV or more), the lower lying minimum remains a minimum when the γ degree of freedom is included. On the other hand, the higher lying minimum becomes a saddle point. When the two minima lie at a depth not differing by more than a couple of MeV, it is likely that a triaxial minimum develops, and the prolate and oblate minima become saddle points. The latter is not a theorem but represents a very likely situation that obviously is prone to exceptions.

IV. CONCLUSIONS

With the aim of obtaining first hints on nuclear phase shape transitions around ^{190}W within the self-consistent Skyrme HF+BCS scheme, we have considered in the present work the PECs of five isotopic chains, namely, Yb, Hf, W, Os, and Pt for $106 \leqslant N \leqslant 122$. Our study has been based on different Skyrme-like energy functionals plus different recipes for pairing correlations, and comparisons have been made with results obtained using the Hartree-Fock-Bogoliubov approximation based on the Gogny interaction.

From the analysis of our results, we conclude that at least in the mass region studied, the PECs are not sensitive to the method employed to solve the HF+BCS equations (three-dimensional Cartesian lattice or deformed harmonic oscillator basis). We also conclude that the qualitative behavior of the energy profiles remains unchanged against changes in the Skyrme and pairing interactions in the sense that the deformations at which the energy minima occur are rather stable. This agrees well with results obtained with other nonrelativistic approximations including those involving the Gogny force, as well as with results obtained within the RMF. However, the spherical energy barriers between the minima are found to be sensitive to the details of the calculations.

As already mentioned, our main intention in this study has been to obtain first hints of nuclear phase shape transitions in the region under discussion. In this context, we find signatures for a transition from prolate to oblate shapes as the number of neutrons increases from $N = 110$ up to $N = 122$ in Yb, Hf, W, and Os isotopes. The lighter isotopes of these nuclei exhibit a rotational behavior that changes gradually toward γ soft as the number of neutrons increases. The transition is found to happen at $N = 116$–118, where the energies of prolate and oblate shapes are nearly degenerate. In the case of Pt, the isotopes considered do not show a rotor behavior, and a prolate shape in the lighter isotopes is not clearly developed yet. Let us also mention that our results agree qualitatively with previous predictions of shape transitions in this mass region.

The role played by triaxiality in the description of ground state properties for nuclei in this mass region has been investigated by calculating β-γ energy contour plots, and in

particular, the energy behavior with the γ variable for fixed values of β corresponding to the axial minima. The analysis of our results shows that the axial prolate and oblate minima, which are well separated by high spherical barriers in the β degree of freedom, are linked very softly in the γ degree of freedom.

Finally, a long list of tasks remains to be undertaken in the near future, and this work can be viewed as a starting point for a more ambitious project. In particular, it will be worth determining the extent to which the results discussed above might be modified by including dynamical correlations beyond the static mean field picture. This is particularly interesting if one notes that at least for some of the considered nuclei, shape coexistence is clearly visible, and therefore it is important to check the role played by symmetry restoration and/or configuration mixing.

ACKNOWLEDGMENTS

This work was partly supported by Ministerio de Educación y Ciencia (Spain) under Contract Nos. FIS2005-00640 and FPA2007-66069.

[1] J. L. Wood, K. Heyde, W. Nazarewicz, M. Huyse, and P. Van Duppen, Phys. Rep. **215**, 101 (1992).
[2] J. Dechargé and D. Gogny, Phys. Rev. C **21**, 1568 (1980).
[3] D. Vautherin and D. M. Brink, Phys. Rev. C **5**, 626 (1972); D. Vautherin, *ibid*. **7**, 296 (1973).
[4] M. Bender, P.-H. Heenen, and P.-G. Reinhard, Rev. Mod. Phys. **75**, 121 (2003).
[5] D. Vetrenar, A. V. Afanasjev, G. A. Lalazissis, and P. Ring, Phys. Rep. **409**, 101 (2005).
[6] J. L. Egido, J. Lessing, V. Martin, and L. M. Robledo, Nucl. Phys. **A594**, 70 (1995).
[7] Zs. Podolyák *et al*., Phys. Lett. **B491**, 225 (2000).
[8] M. Caamaño *et al*., Eur. Phys. J. A **23**, 201 (2005).
[9] P. M. Walker and F. R. Xu, Phys. Lett. **B635**, 286 (2006).
[10] P. M. Walker and G. D. Dracoulis, Nature (London) **399**, 35 (1999).
[11] R. F. Casten and B. M. Sherrill, Prog. Part. Nucl. Phys. **45**, S171 (2000).
[12] J. Jolie and A. Linnemann, Phys. Rev. C **68**, 031301(R) (2003).
[13] *Table of Isotopes: 1999 Update with CD-ROM*, 8th ed., edited by R. B. Firestone, C. M. Baglin, and S. Y. Frank Chu (Wiley, New York, 1999).
[14] H. Mach, Phys. Lett. **B185**, 20 (1987).
[15] C. Y. Wu *et al*., Nucl. Phys. **A607**, 178 (1996).
[16] W. Nazarewicz, M. A. Riley, and J. D. Garrett, Nucl. Phys. **A512**, 61 (1990).
[17] C. Wheldon *et al*., Phys. Rev. C **63**, 011304(R) (2000).
[18] Z. Naik, B. K. Sharma, T. J. Jha, P. Arumugam, and S. K. Patra, Pramana **62**, 827 (2004).
[19] R. Fossion, D. Bonatsos, and G. A. Lalazissis, Phys. Rev. C **73**, 044310 (2006).
[20] P. D. Stevenson, M. P. Brine, Z. Podolyak, P. H. Regan, P. M. Walker, and J. R. Stone, Phys. Rev. C **72**, 047303 (2005).
[21] P. Stevenson, M. R. Strayer, and J. R. Stone, Phys. Rev. C **63**, 054309 (2001).
[22] P. Bonche, H. Flocard, and P.-H. Heenen, Comput. Phys. Commun. **171**, 49 (2005).
[23] P. Ring and P. Schuck, *The Nuclear Many-Body Problem* (Springer, Berlin, 1980).
[24] M. Beiner, H. Flocard, N. Van Giai, and P. Quentin, Nucl. Phys. **A238**, 29 (1975).
[25] E. Chabanat, P. Bonche, P. Haensel, J. Meyer, and R. Schaeffer, Nucl. Phys. **A635**, 231 (1998).
[26] J. F. Berger, M. Girod, and D. Gogny, Nucl. Phys. **A428**, 23c (1984).
[27] P. Bonche, H. Flocard, P.-H. Heenen, S. J. Krieger, and M. S. Weiss, Nucl. Phys. **A443**, 39 (1985).
[28] D. Baye and P.-H. Heenen, J. Phys. A **19**, 2041 (1986).
[29] J. Terasaki, P.-H. Heenen, H. Flocard, and P. Bonche, Nucl. Phys. **A600**, 371 (1996).
[30] C. Rigollet, P. Bonche, H. Flocard, and P.-H. Heenen, Phys. Rev. C **59**, 3120 (1999).
[31] M. Bender, G. F. Bertsch, and P.-H. Heenen, Phys. Rev. C **73**, 034322 (2006).
[32] B. Sabbey, M. Bender, G. F. Bertsch, and P.-H. Heenen, Phys. Rev. C **75**, 044305 (2007).
[33] H. Flocard, P. Quentin, A. K. Kerman, and D. Vautherin, Nucl. Phys. **A203**, 433 (1973).
[34] J. Meng, W. Zhang, S. G. Zhou, H. Toki, and L. S. Geng, Eur. Phys. J. A **25**, 23 (2005).
[35] N. Tajima, S. Takahara, and N. Onishi, Nucl. Phys. **A603**, 23 (1996).
[36] P. Sarriguren, O. Moreno, R. Alvarez-Rodriguez, and E. M. de Guerra, Phys. Rev. C **72**, 054317 (2005).
[37] R. Rodriguez-Guzman and P. Sarriguren, Phys. Rev. C **76**, 064303 (2007).
[38] J. L. Egido, L. M. Robledo, and R. Rodriguez-Guzman, Phys. Rev. Lett. **93**, 082502 (2004).
[39] S. Hilaire and M. Girod, Hartree-Fock-Bogoliubov results based on the Gogny force, www-phynu.cea.fr.
[40] G. Audi, O. Bersillon, J. Blachot, and A. H. Wapstra, Nucl. Phys. **A729**, 3 (2003).
[41] G. A. Lalazissis, S. Raman, and P. Ring, At. Data Nucl. Data Tables **71**, 1 (1999).
[42] P. Raghavan, At. Data Nucl. Data Tables **42**, 189 (1989); N. J. Stone, Table of Nuclear Moments (2001) www.nndc.bnl.gov/nndc/stone_moments.
[43] S. Raman, C. W. Nestor, Jr., and P. Tikkanen, At. Data Nucl. Data Tables **78**, 1 (2001).
[44] E. Moya de Guerra, Phys. Rep. **138**, 293 (1986).